

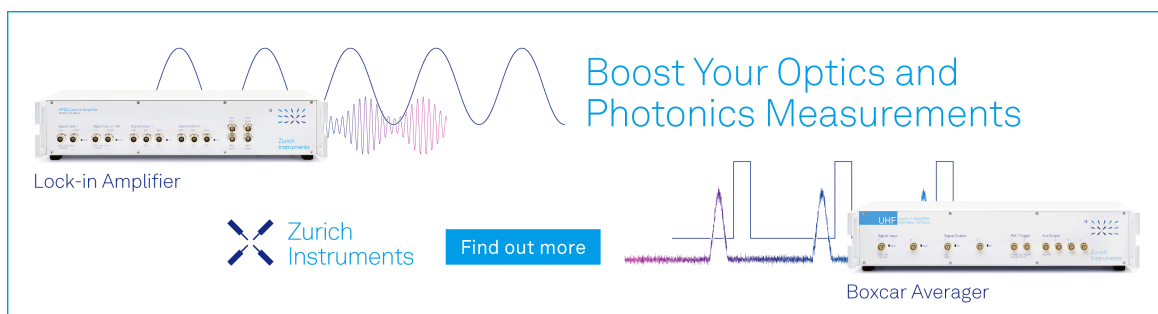
RESEARCH ARTICLE | JUNE 15 2023

High-level studies of the singlet states of quadricyclane, including analysis of a new experimental vacuum ultraviolet absorption spectrum by configuration interaction and density functional calculations

Michael H. Palmer ; Søren Vrønning Hoffmann ; Nykola C. Jones ; Marcello Coreno ; Monica de Simone ; Cesare Grazioli ; R. Alan Aitken ; Coralysse Peureux



J. Chem. Phys. 158, 234303 (2023)
<https://doi.org/10.1063/5.0151758>



Boost Your Optics and Photonics Measurements

Lock-in Amplifier

Zurich Instruments

Find out more

Boxcar Averager

High-level studies of the singlet states of quadricyclane, including analysis of a new experimental vacuum ultraviolet absorption spectrum by configuration interaction and density functional calculations

Cite as: *J. Chem. Phys.* **158**, 234303 (2023); doi: 10.1063/5.0151758

Submitted: 24 March 2023 • Accepted: 30 May 2023 •

Published Online: 15 June 2023



View Online



Export Citation



CrossMark

Michael H. Palmer,^{1,a)} Søren Vrønning Hoffmann,^{2,b)} Nikola C. Jones,^{2,c)} Marcello Coreno,^{3,d)}
Monica de Simone,^{4,e)} Cesare Grazioli,^{4,f)} R. Alan Aitken,^{5,g)} and Coralyse Peureux^{5,h)}

AFFILIATIONS

¹School of Chemistry, University of Edinburgh, Joseph Black Building, David Brewster Road, Edinburgh EH9 3FJ, Scotland, United Kingdom

²ISA, Department of Physics and Astronomy, Aarhus University, Ny Munkegade 120, DK-8000 Aarhus C, Denmark

³ISM-CNR, Istituto di Struttura della Materia, LD2 Unit, 34149 Trieste, Italy

⁴IOM-CNR, Istituto Officina dei Materiali, Basovizza SS-14, Km 163.5, 34149 Trieste, Italy

⁵School of Chemistry, University of St Andrews, North Haugh, St Andrews, Fife KY16 9ST, Scotland, United Kingdom

^{a)} Author to whom correspondence should be addressed: m.h.palmer@ed.ac.uk

^{b)} Electronic mail: vronning@phys.au.dk

^{c)} Electronic mail: nykj@phys.au.dk

^{d)} Electronic mail: marcello.coreno@elettra.eu

^{e)} Electronic mail: desimone@iom.cnr.it

^{f)} Electronic mail: grazioli@ism.cnr.it

^{g)} Electronic mail: raa@st-andrews.ac.uk

^{h)} Electronic mail: coralyse.peureux@laposte.net

ABSTRACT

A synchrotron-based vacuum ultraviolet absorption spectrum (VUV) of quadricyclane (QC) is reported with energies up to 10.8 eV. Extensive vibrational structure has been extracted from the broad maxima by fitting short energy ranges of the VUV spectrum to high level polynomial functions and processing the regular residuals. Comparison of these data with our recent high-resolution photoelectron spectral of QC showed that this structure must be attributed to Rydberg states (RS). Several of these appear before the valence states at higher energies. Both types of states have been calculated by configuration interaction, including symmetry-adapted cluster studies (SAC-CI) and time dependent density functional theoretical methods (TDDFT). There is a close correlation between the SAC-CI vertical excitation energies (VEE) and both Becke 3-parameter hybrid functional (B3LYP), especially Coulomb-attenuating method-B3LYP determined ones. The VEE for several low-lying s-, p-, d-, and f-RS have been determined by SAC-CI and adiabatic excitation energies by TDDFT methods. Searches for equilibrium structures for $1^{1,3}A_2$ and 1^1B_1 states for QC led to rearrangement to a norbornadiene structure. Determination of the experimental 0^0 band positions, which show extremely low cross-sections, has been assisted by matching features in the spectra with Franck–Condon (FC) fits. Herzberg–Teller (HT) vibrational profiles for the RS are more intense than the FC ones, but only at high energy, and are attributed to up to ten quanta. The vibrational fine structure of the RS calculated by both FC and HT procedures gives an easy route to generating HT profiles for ionic states, which usually require non-standard procedures.

© 2023 Author(s). All article content, except where otherwise noted, is licensed under a Creative Commons Attribution (CC BY) license (<http://creativecommons.org/licenses/by/4.0/>). <https://doi.org/10.1063/5.0151758>

I. INTRODUCTION

Recently, we reported synchrotron based, high-resolution photoelectron spectral (PES) for both quadricyclane (QC, 1) and norbornadiene (NBD, 2) molecules as shown in Fig. 1.¹ This was followed by a vacuum ultraviolet (VUV) absorption spectral study of NBD.² The PES of 1 and 2 reveal the existence of different radical cation states (QC⁺ and NBD⁺).¹ Similarly, the hyperfine coupling patterns, established by the application of the chemically induced dynamic nuclear polarization (CIDNP) technique, resulted in the observation of discrete polarization patterns for these two radical cations. In contrast, matrix-isolation studies give only a single species from both QC and NBD molecules, while mass spectrometry gives identical fragmentation patterns. Both QC⁺ and NBD⁺ were discussed previously.¹

QC and NBD have a significant joint history, in the search for methods of solar energy storage.^{3–6} Photo-absorption by NBD generates QC, in what is termed molecular solar thermal energy storage (MOST); the QC strain energy is liberated in a subsequent stage regenerating NBD. Since the main intensity of solar wavelengths lies between 300 and 700 nm, substituents are necessary on both NBD and QC moieties to shift the absorption to longer wavelengths. This is achieved by having both electron donating and accepting groups present on both the QC and the NBD units, leading to a push-pull mechanism.¹ The onset wavelength for absorption by NBD is 267 nm, but the absence of a chromophore in the structure of QC itself has resulted in no reports of its UV absorption.

The molecular structure of QC has been determined by both gas phase electron diffraction (ED)⁷ and microwave spectroscopy,⁸ the structure appears to have classical cyclopropane and other rings.^{7,8} Rydberg states (RS) are particularly important for a saturated system like QC; σ^* -valence states are likely to lie at higher energies than, for example, $\pi\pi^*$ -states in unsaturated molecules, such as NBD. Rudakov and Weber (R & W)⁹ focused on Rydberg states for the joint system QC + NBD. QC on irradiation with 208 nm photons

generates 3s and 3p Rydberg states. Their QC spectral analysis⁹ uses a time-delayed second laser at 416 nm, which causes photoionization with excess vibrational energy. The resulting large amplitude motion allows the QC skeleton to rearrange to that of NBD. The binding energy (BE) of the electron in its Rydberg state was ionized by the third photon, and its kinetic energy was measured. Three-photon resonant multiphoton ionization (REMPI), followed by one-color ionization spectra with 416 nm (2.980 eV) photons, was used to observe the 3s state and the two (non-zero intensity) 3p-Rydberg states. The binding energy (BE) relative to the ionic state was 2.88, 2.29, and 2.24 eV for the 3s and two 3p states, respectively.⁹ This BE term differs from conventional usage of the ionization energy (IE) for Rydberg states as used here in the following equation:

$$BE = IE - E = R/(n - \delta)^2, \quad (1)$$

$$(n^2 - 2n\delta + \delta^2) = R/(IE - E). \quad (2)$$

The BE is just the term: $R/(n - \delta)^2$ in Eq. (1), where R is the Rydberg constant (13.61 eV), n is the principal quantum number and δ is the quantum defect. The IE used in both Eqs. (1) and (2) (where the terms have been rearranged) is strictly the adiabatic term (AIE), which is applicable when the PES vibrational structure is well determined. However, many polyatomic molecules show poorly resolved ionization spectra so that the vertical (VIE) term is often used instead. This applied to R & W⁹ who used an early VIE¹⁰ of 8.33 eV as their AIE. For consistency with R & W, we also use the VIE for some of our studies, but our value after ten vibrational intervals from the onset gave 8.363 eV, with the AIE (0–0 band) for QC at 7.671 eV.¹ This leads to the substantial difference between VIE and AIE of 0.692 eV.

We now present the first wide scan vacuum ultraviolet (VUV) absorption spectrum for QC following our previous studies on NBD² and cycloheptatriene (CHT).¹¹ We expose detailed vibrational structure in what appears to be a relatively featureless VUV spectrum, by numerical fitting of local energy ranges of the UV and VUV spectrum to polynomial functions and processing the regular residuals. We will show, in Sec. III, that this vibrational structure is effectively identical to that for the ionic state of QC and, thus, indicates the presence of Rydberg states at the onset of QC UV absorption.

We provide a theoretical analysis up to the coupled cluster (CC) level, which has been claimed to be both the “gold and platinum standard” for electronic structure calculations.^{12,13} Thus, our study allows the correlation of theory with experiment at a more rigorous level than is currently available. As with CHT and NBD previously, we analyze the vibrational structure in the VUV spectrum of QC in a detailed manner. Our adiabatic theoretical studies enable both Franck-Condon (FC) and Herzberg-Teller (HT) methods to be performed. Correlation of the theoretical envelopes with the experimental spectra assists identification of the 0⁰ band origins and,

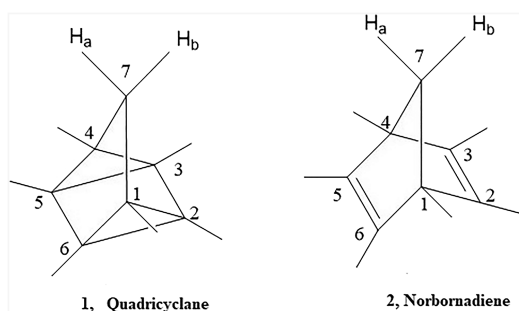


FIG. 1. The quadricyclane (1, QC) and norbornadiene (2, NBD) structures. Classical bond switching between the two systems occurs during UV excitation. For simplicity, H atoms are unmarked for the ring system moieties.

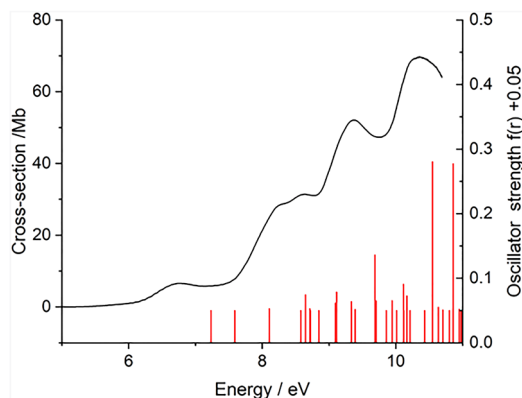


FIG. 2. The VUV absorption spectrum of quadricyclane with SAC-CI calculated valence state energies. The energies for this theoretical series do not explain the lower onset of the spectrum, leading to the conclusion that Rydberg states are dominant, especially in the low VEE energy range. This is demonstrated in Fig. 3. To show the positions of the optically forbidden 1A_2 states, the oscillator strengths have been increased by 0.05 units.

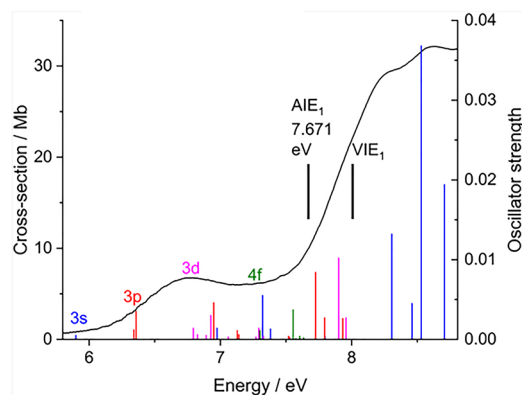


FIG. 3. The VUV absorption spectrum of quadricyclane with CAM-B3LYP calculated Rydberg states using very diffuse functions of s, p, d, and f symmetry. The adiabatic ionization energy (AIE_1) for QC is at 7.671 eV and was assigned to the X^2B_2 state in Ref. 1. The corresponding vertical ionization (VIE_1) was assigned to the fourth member of the progression, with a vibration frequency of 663 cm^{-1} , at 8.005 eV. Some higher intensity valence states appear above 8.3 eV.

hence, adiabatic excitation energies (AEE) for the electronic states. Our study also includes the generation of the theoretical vibrational structure for Rydberg states at the density functional theoretical (DFT) level, having each of s-, p-, d-, or f-types of excitations.

II. METHODS

QC has CAS registry number 278-06-8, with numbering as in Fig. 1. It has been systematically named both as tetracyclo [2.2.1.0^{2,6}.0^{3,5}] heptane and tetracyclo [3.2.0.0^{2,7}.0^{4,6}] heptane under International Union of Pure and Applied Chemistry (IUPAC) rules.

A. Synthesis

QC was prepared from NBD by irradiation using a water-cooled 400 W medium-pressure mercury discharge lamp with acetophenone as a photosensitizer; further details were given previously.¹ Although considerable care was taken to free the QC from NBD contamination, the VUV absorption samples showed about 1% NBD remained in the spectrum of QC. In practice, this assisted interpretation of the onset of the QC spectrum; since both compounds show vibrational structure in the 5.5–6.0 eV region, the peak maxima do not correspond. Indeed, several minima for QC match with maxima for NBD.

B. The VUV absorption spectrum of QC

This was measured in the gaseous phase at 25 °C on the AU-UV beamline of the ASTRID2 synchrotron (in Aarhus, Denmark) using methods described previously.¹⁴ The full UV + VUV spectrum was covered by 3681 data points over the range 330 nm (3.857 eV) to 116 nm (10.751 eV). These data are separated by 0.05 nm for most of the spectral range; but by 0.1 nm from 270 nm to higher wavelengths. The photon resolution is 0.08 nm over the operational range of the grating; this corresponds to 7, 3, and 1 meV at the high, mid, and low energy range, respectively.

The spectrum is discussed in detail below; however, here, we note that the wide scan quadricyclane VUV spectrum for the energy range up to 10.8 eV, shown in Fig. 2, has a slow onset close to 5 eV (as demonstrated in Figs. 3 and 4) with broad peaks occurring at 6.77(1), 8.62(1), 9.38(1), and 10.34(1) eV, with a point of inflexion at 8.30(1) eV. Minor undulations, which occur between 6.0 and 7.2 eV, are discussed later. Throughout this study, errors are in parentheses. The spectrum, shown in Fig. 2, has been corrected to remove ~1% contamination by NBD.

Figure 2 also exhibits the most rigorous theoretical vertical excitation energies from the present SAC-CI studies, which are given in Table I. These excitation energies cannot explain the UV region shown since the calculated onset of absorption is some 1.2 eV

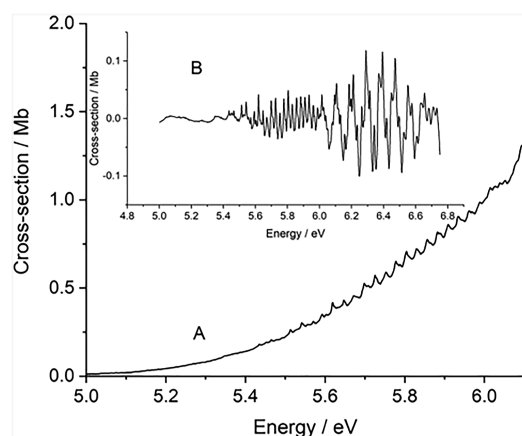


FIG. 4. The raw QC absorption data shown in A; after fitting to a ninth-order polynomial, this gives the regular residuals shown in B. The vibrational sequence in the range 5.5–6.0 eV is the 3s-Rydberg state. The more complex multiplet between 6.0 and 6.8 eV is the two allowed 3p-Rydberg states.

TABLE I. A comparison of the vertical excitation energies for the lower singlet valence states of quadricyclane using the SAC-CI coupled cluster and CAM-B3LYP density functional methods at the 6-311G (d, p) basis set level, where more than one configuration is shown, and these are in declining density. However, a single term merely shows dominance, not exclusivity. Unexpectedly, we find that there is a close correlation between these two sets of data. Using abbreviated terminology, there is a linear relationship: CAM = 0.835(28)*SAC + 1.042(271) with a correlation coefficient (CC) of 0.974; standard deviations (SD) are in parentheses.

State symmetry	SAC-CI (eV)	CAM-B3LYP (eV)	Excitation	State symmetry	SAC-CI (eV)	CAM-B3LYP (eV)	Excitation
1^1B_2	7.23	7.16	$5b_28a_1^*$	4^1A_2	9.86	9.16	$2a_29a_1^*$
1^1A_2	7.59	7.22	$5b_25b_1^*$	3^1B_1	9.71	9.20	$2a_26b_2^* + 4b_19a_1^*$
1^1A_1	8.11	7.87	$5b_26b_2^*$	5^1A_2	10.01	9.36	$5b_26b_1^* + 2a_29a_1^*$
2^1B_2	8.65	8.08	$5b_29a_1^*$	3^1B_1	9.94	9.41	$4b_19a_1^* - 2a_26b_2^*$
2^1A_2	8.58	8.32	$5b_26b_1^* + 2a_28a_1^*$	5^1B_2	10.21	9.51	$5b_211a_1^*$
2^1A_1	8.71	8.42	$5b_27b_2^* - 5b_26b_2^*$	6^1A_2	10.12	9.61	$4b_16b_2^* - 2a_210a_1^*$
3^1A_2	8.72	8.42	$2a_28a_1^* - 5b_26b_1^*$	4^1B_1	10.17	9.62	$2a_27b_2^* - 2a_26b_2^*$
3^1B_2	9.09	8.44	$5b_210a_1^* - 2a_25b_1^*$	5^1A_1	10.11	9.76	$7a_111a_1^*$
1^1B_1	8.85	8.57	$5b_23a_2^* + 4b_18a_1^*$	6^1B_2	10.71	9.79	$2a_26b_1^* + 5b_26b_1^*$
4^1B_2	9.33	8.62	$2a_25b_1^* + 5b_210a_1^*$	7^1A_2	10.43	9.81	$4b_17b_2^* + 2a_210a_1^*$
2^1B_1	9.11	8.69	$5b_23a_2^* + 4b_18a_1^*$	5^1B_1	10.64	9.90	$7a_15b_1^*$
3^1A_1	9.39	8.84	$4b_15b_1^* - 5b_27b_2^*$	6^1A_1	10.55	9.94	$2a_23a_2^* + 4b_16b_1^*$
4^1A_1	9.69	9.09	$5b_28b_2^* + 4b_15b_1^*$	6^1B_1	10.86	10.21	$4b_110a_1^*$

higher than the experiment. Thus, the onset must be a result of the Rydberg states given in Table II; this is confirmed by Fig. 3, which shows the Rydberg states described below. These cover the onset energy range satisfactorily and are discussed separately. Conversely, the higher energy region of the spectrum shown must relate to the calculated valence states in Table I. Both are discussed below (Fig. 4).

C. Theoretical methods

The Gaussian suite (G-16)¹⁵ was used for the calculation of vertical and adiabatic excitation energies (VEE and AEE) for both

valence and Rydberg states, as well as vibrational analysis^{16–18} and symmetry-adapted cluster configuration interaction (SAC-CI) studies.^{19–23} SAC-CI studies are our most rigorous theoretical determinations of the excited state sequence; however, in our hands, this method is an “excitation energy only” procedure since the available G-16 version of the code does not give us the facility to use the wave-functions for vibrational or other analyses. Thus, a second method of excited state energy determination was essential; time-dependent density functional theory (TDDFT),^{24–26} a single excitation configuration interaction (CI) method, was particularly suitable since it enabled equilibrium structures and harmonic frequencies for both valence and Rydberg states to be determined,

TABLE II. A comparison of the vertical excitation energies for the lower singlet s-Rydberg states of quadricyclane using the SAC-CI coupled cluster method at the 6-311G (d, p) basis set level. Compared with the results in Table I, energies of comparable states are lowered by ~1.2 eV, as a result of the Rydberg functions, but are still not sufficiently low to account for the spectral onset.

Symmetry	PQN sequence	Energy (eV)	f(r)	Symmetry	PQN sequence	Energy (eV)	f(r)
1^1B_2	3	6.009	0.001	3^1B_2	7	7.60	0.000
1^1A_2	3	6.381	0.000	1^1B_1	3	7.62	0.000
1^1A_1	3	6.469	0.003	3^1B_2	5	7.63	0.006
1^1B_2	3	6.492	0.002	2^1B_2	5	7.66	0.000
1^1B_2	4	7.070	0.000	3^1A_2	5	7.81	0.000
2^1B_2	4	7.180	0.004	3^1A_1	5	7.98	0.009
2^1B_2	4	7.215	0.002	1^1A_1	3	8.13	0.000
1^1B_2	5	7.343	0.000	3^1B_2	6	8.19	0.000
2^1A_2	4	7.349	0.000	2^1A_1	4	8.62	0.013
2^1A_1	4	7.427	0.002	2^1B_1	4	8.81	0.002
3^1B_2	5	7.455	0.000	3^1A_1	5	8.91	0.027
2^1B_2	6	7.583	0.000	3^1B_1	5	9.14	0.021

and AEE for several states of each symmetry. The wavefunctions were directly compatible with the FC and HT software for vibrational analysis.^{16–18} The primary density functional used was a long-range-corrected version of the Becke 3-parameter hybrid functional (B3LYP),²⁷ described as the Coulomb-attenuating method (CAM-B3LYP).²⁸

Rydberg States (RS) were generated computationally by use of very diffuse Gaussian-type basis functions; exponents: 0.021, 0.008, and 0.0026 were added to the strictly valence TZVP basis set.^{30,31} Since Rydberg functions must be mounted on atomic centers in G-16, and their atomic site was listed first in the geometric specification, the standard structural numbering in Fig. 1 was rearranged in the Rydberg state calculations with C₇ relabeled as C₁. This is reproduced in the supplementary material as SM1.

The work described here was performed using the 6-311G (d, p) basis set.²⁹ For *nd* and *nf* states, the 5d and 7f options were implemented, thereby removing interference from the implicit *s*-functions through the elimination of terms such as $(d_x^2 + d_y^2 + d_z^2) = d_r^2$.

We use valence shell numbering of molecular orbitals, with doubly occupied MOs up to 7a₁, 5b₂, 4b₁, and 2a₂; the core MOs, excluded from the CI studies, consist of 3a₁ + 2b₂ + 1b₁ + 1a₂. It is necessary to discuss the singlet state manifolds prior to the use of their results in the interpretation of the VUV spectrum of QC.

III. RESULTS

A. The ground state bonding of the quadricyclane molecule

Electron density plots of the highest group of the occupied MOs (23–25), together with the lowest virtual orbitals (VMOs, 26–28) are shown in the supplementary material as SM2. These are involved in many of the lowest valence states for QC, including those given in Table I. We give additional detail concerning the electron density distribution in QC using the Atoms in Molecules (AIM) approach.³² In this procedure, integration of the electron density along all internuclear axes, and also across the centers of each ring, is performed using the QTAIM package.³³ This shows that the electron density declines to a minimum along all C–H and C–C bonds as well as at the centers of all rings. These minima, known as critical points (CP),³² are shown in the supplementary material under SM3. Since each CP lies much closer to the H than the C atoms, all the C–H bonds are polarized in the sense C^{δ−}–H^{δ+}. In contrast, the C–C bonds have a CP close to their midpoint. QC has a very low dipole moment,⁸ and $\mu = \mu_b = 0.01989$ (18) D has been determined from Stark effect measurements. This must be largely attributable to the C–H polarization of the seven-CH₂ group.

B. The theoretical singlet valence states manifold

Unexpectedly, Table I shows that the singlet states determined by the CAM-B3LYP method gave a close energy correlation with those from the (much more rigorous) coupled cluster SAC-CI method. This correlation was performed by only considering like-with-like comparisons, such as A₁ with A₁, etc., and having similar excitation types; it does not just compare two sets of ascending numbers. The two vertical excitation energy sequences by symmetry are not identical, but the differences are generally small fractions of 1 eV.

Given the width associated with UV + VUV absorptions, where the lowest mode (39) for QC is 368 cm^{−1}, as discussed below, but with most modes higher than 1000 cm^{−1}, these small differences between state energy separations will lead to many overlaps of singlet state vibrational sequences, with consequent loss of observed structure. Thus, the SAC-CI and CAM-B3LYP state energies can be used interchangeably for most purposes. In detail, the correlation shows that the CAM-B3LYP excitation energy levels are substantially lower (17%) than those of SAC-CI but offset by around 1.0 eV. The correlation is shown in the supplementary material as SM5. Subsequently, it appeared that several other DFT functionals gave related correlations,³⁴ as described in the supplementary material as SM4.

All the singlet states, given in Table I, have several leading configurations, and these include symmetric and antisymmetric combinations. The highest occupied molecular orbital (HOMO, 5b₂) is involved as the leading term in the ten lowest excited states and some other states.

The next two doubly occupied molecular orbitals (DOMOs), 2a₂ and 4b₁, also appear in groups of higher excited states; these three DOMOs and the lowest three virtual orbitals shown in SM2 cover the energy levels populated in Table I. The first leading term involving the next DOMO (7a₁) lies at calculated energy close to 9.5 eV. Only 20 valence states up to 11 eV have an oscillator strength $f(r) > 0.01$ units; only 8 lie above $f(r) > 0.05$, while only 2 of these have $f(r) > 0.1$ units. The highest occupied molecular orbital (HOMO) to the lowest unoccupied molecular orbital (LUMO) excitation (5b₂8a₁^{*}, X¹B₂) is typical, with an extremely low oscillator strength [$f(r)$ 0.0010]. The absence of dominant peaks in the VUV spectrum is readily interpreted in these terms. Up to this stage, the theoretical determination of the excited states has all been performed at the X¹A₁ ground state equilibrium structure. In Secs. III C–III E, concerned with Rydberg states, all theoretical work was performed either at the equilibrium structure or at the structure of the lowest ionic state X²B₂, as determined previously.¹ Since Rydberg and their limiting ionic state share ionic state structures, this is a suitable choice for non-optimal structures.

C. Rydberg state calculations

These were performed separately with each of the SAC-CI and DFT modules. As in several of our earlier studies,^{1,2,11,14} the Rydberg basis functions populate the lowest energy group of virtual molecular orbitals (VMOs) at the Hartree–Fock level; this is relative to the corresponding valence states whose orbitals move to higher energy positions. The 3s, 4s, and 5s Rydberg states occupy VMOs 26–28. In all the evaluated Rydberg states, these 3s, 4s, and 5s VMOs occur as linear combinations of the input Gaussian orbital. Similar positions occur for p-, d-, and f-Rydberg orbitals.

The Rydberg state vertical excitation energy results, performed at the equilibrium structure of the ground state, are unscaled in energy, and given in Table II. In principle, these can be extrapolated to the VEE, but the three Rydberg functions can only generate states with principal quantum numbers 3, 4, and 5. Such results are shown in the supplementary material under SM5.

Several CAM-B3LYP calculated adiabatic excitation energy Rydberg states are given in Table III. It is impracticable to determine

TABLE III. TZVPR basis set equilibrium structures for Rydberg states with s, p, d, and f spherical harmonics.

State	Symmetry	Rydberg state energy (eV)		State	Symmetry	Rydberg state energy (eV)	
		TDDFT	Corrected			TDDFT	Corrected
3s	1 ¹ B ₂	4.29	5.51	3d	1 ¹ B ₁	5.24	6.99
4s	2 ¹ B ₂	5.41	6.64	4d	2 ¹ B ₁	5.80	7.56
5s	3 ¹ B ₂	5.86	7.10	5d	3 ¹ B ₁	6.48	8.25
3p	1 ¹ B ₂	4.89	5.92	4f	1 ¹ B ₁	5.72	7.46
3p	1 ¹ A ₁	4.94	5.97	5f	2 ¹ B ₁	6.07	7.82
4p	2 ¹ A ₁	5.59	6.82	6f	3 ¹ B ₁	7.08	8.80
5p	3 ¹ A ₁	6.53	7.56				

TABLE IV. All harmonic frequencies participating in the Franck–Condon and Herzberg–Teller modes for the 1¹B₂ state in Tables V and VI. The frequencies are labeled with the spectroscopic modes a₁ < a₂ < b₁ < b₂.

Mode	Symmetry a ₁	Mode	Symmetry a ₂	Mode	Symmetry b ₁	Mode	Symmetry b ₁
1	3381	13	3385	21	3389	30	3390
2	3339	14	1380	22	3294	31	3344
3	3232	15	1292	23	1449	32	1520
4	1623	16	1189	24	1202	33	1418
5	1514	17	1094	25	1077	34	1384
6	1474	18	873	26	1073	35	1126
7	1146	19	689	27	908	36	1011
8	1114	20	441	28	811	37	871
9	979			29	453	38	820
10	949					39	368
11	802						
12	693						

equilibrium structures for all the lower Rydberg states; however, we have obtained equilibrium structures and harmonic frequencies for all three of the 5b₂ excitations to 3s, 4s, and 5s Rydberg states; the structures are effectively identical, as are the harmonic frequencies. These structures will be almost identical to that of the lowest ionic state, as is assumed for Rydberg states. The CAM-B3LYP energies of the calculated structures are superimposed on the onset of the VUV spectrum in Fig. 3. The Rydberg states for each of the Rydberg s-, p-, d-, and f-energies are displayed in distinct colors, together with our recently determined adiabatic and vertical ionization energies. The Rydberg states give an interpretation of the spectral onset. Overall, we interpret the VUV spectrum as a complex mixture, with Rydberg states at the onset, and valence states dominating the higher energy range of Fig. 2. In our experience, valence states can show a wide range of intensities, while Rydberg states are universally weak, as is seen here.

The CAM-B3LYP density functional energy results, given in Table III, were each determined by single calculations as is normal in G-16. In that suite, the excited state is correctly found, but the ground state is determined at this excited state structure. We require the normal spectroscopic convention, where both

ground and excited states are determined at their equilibrium structures. This leads to essential corrections to the G-16 energies, to bring the results for the adiabatic excitation energies into alignment with spectroscopic standard usage. Each pair of “TDDFT” and “Corrected” energies in Table III is independently determined. However, the corrected energies in Table III give a close linear correlation to the uncorrected series in this instance; this is not an automatic requirement, but merely pragmatic. We find $E_{\text{Corrected}} = 1.017(34) * E_{\text{TDDFT}} + 1.606(194)$ eV, where the standard errors (SE) are in parentheses and the CC is 0.987. Thus, in general, the Rydberg state energies after correction are ~1.61 eV higher than those initially determined. The need to make these re-evaluations is obvious.

The vertical VIE for quadricyclane are 8.199 (X²B₂), 9.608 (1²A₂), 9.946 (1²B₁), and 10.914 eV (1²A₁) using data from our previous study.¹ Comparing the data from Tables I–III leads to the conclusion that the lowest Rydberg state, 5b₂3s, is lower in energy by ~0.4 eV than the corresponding valence state. The 3p states, shown in Fig. 3, also involving 5b₂ excitation, occur a further ~0.5 eV higher in energy. The full set of energies shown in Fig. 3 is listed in the supplementary material as SM6.

TABLE V. The Franck–Condon analysis of the lowest Rydberg state ($5b_23s$) using the TZVPR basis set. The modes shown in the first and fourth columns are the a_1 modes. The complete onset of the lowest set of vibrational states is shown in columns 1–3. The most intense bands are in columns 4–6.

Energy (cm^{-1})	Relative intensity	Modes excited + quanta	Energy (cm^{-1})	Relative intensity	Modes excited + quanta
0	0.0078	0^0	4668	1.824	$10^2 12^4$
693	0.0396	12^1	4777	1.769	$10^2 11^1 12^3$
802	0.0080	11^1	4924	1.811	$10^3 12^3$
949	0.0276	10^1	5361	1.865	$10^2 12^{12}$
1385	0.1290	12^2	5617	2.410	$10^3 12^4$
1494	0.0376	$11^1 12^1$	5873	1.798	$10^4 12^3$
1641	0.1849	$10^1 12^1$	6162	1.973	$10^2 11^1 12^{12}$
1750	0.0247	$9^1 11^1$	6419	2.393	$10^3 11^1 12^4$
1807	0.0209	$8^1 12^1$	6732	1.758	$8^1 10^3 12^4$
1898	0.0643	10^2	6840	1.518	$8^1 10^3 11^1 12^3$
2063	0.0143	$8^1 10^1$	7424	1.762	$8^1 10^3 12^{12}$
2078	0.1834	12^3	8226	1.759	$8^1 10^3 11^1 12^{12}$

TABLE VI. The Herzberg–Teller analysis of the $5b_23s$ Rydberg state. The modes shown in columns 1–3 are the complete onset, as in Table V, including non-symmetric modes of a_2 , b_1 , and b_2 symmetry. The most intense modes are in columns 4–6.

Energy (cm^{-1})	Relative intensity	Modes excited + quanta	Energy (cm^{-1})	Relative intensity	Modes excited + quanta
0	0.0007	0^0	5037	6.177	$10^2 12^4 39^1$
1061	0.1357	$5^1 39^1$	5729	6.432	$10^2 12^{12} 39^1$
1317	0.0941	$12^1 39^1$	5985	8.293	$10^3 12^4 39^1$
1754	0.4454	$5^2 39^1$	6146	6.090	$10^2 11^1 12^3 39^1$
1862	0.1282	$6^1 5^1 39^1$	6242	6.175	$10^4 12^3 39^1$
2010	0.6376	$12^1 5^1 39^1$	6293	6.114	$10^3 12^3 39^1$
2119	0.0839	$12^1 6^1 39^1$	6531	6.745	$10^2 11^1 12^{12} 39^1$
2175	0.0709	$18^1 5^1 39^1$	6678	5.708	$10^3 12^{12} 39^1$
2258	0.0943	$10^1 5^2$	6787	8.159	$10^3 11^1 12^4 39^1$
2266	0.2214	$12^2 39^1$	6838	5.873	$10^2 11^1 12^4 39^1$
2432	0.0483	$18^1 12^1 39^1$	6953	5.622	$18^1 10^2 11^1 12^4 39^1$
2443	0.1250	$12^1 6^1 5^1$	7043	5.694	$10^4 11^1 12^3 39^1$
2446	0.6223	$5^3 39^1$	7100	5.961	$18^1 10^3 12^4 39^1$
2490	0.1160	$5^2 39^3$	7627	5.730	$10^4 12^{12} 39^1$
2514	0.1349	$12^1 10^1 5^1$	7793	6.094	$18^1 12^3 5^5 39^1$
2555	0.4620	$6^1 5^2 39^1$	8049	5.800	$18^1 12^4 5^4 39^1$
2664	0.0839	$6^2 5^1 39^1$	8594	6.024	$18^1 12^3 6^1 5^5 39^1$

D. Vibrational analysis of the Rydberg states of quadricyclane under TDDFT conditions

The full set of symmetric and non-symmetric harmonic frequencies for the lowest excited state, 1^1B_2 , is given in Table IV since we present both Franck–Condon (FC) and Herzberg–Teller (HT) analyses of some states below. The frequencies are listed in the standard spectroscopic mode convention where all $a_1 < a_2 < b_1 < b_2$ frequencies are given. It is important to note that the numbering used in both G-16 and the Pisa vibrational analysis software is in ascending frequency sequence, irrespective of symmetry. For example, in Table IV, 368 cm^{-1} is mode 39 under the

standard labeling, but in the ascending sequence by frequency is mode 1.

The FC analysis of the lowest Rydberg excited state (1^1B_2) is given in Table V, with the corresponding HT analysis in Table VI. In these and the following tables, we give the complete onset of the vibrational envelope to show the nature of the processes. We also show the most important combination bands in terms of intensity. In FC processes, only odd quanta of a_1 modes are stimulated, while nonsymmetric modes can only occur with even quanta. Several fundamentals occur but with weak intensity. The most intense FC modes are overtones and multiple combinations of up to ten

combination bands, which have the highest numerical intensity and are the strongest peaks in the theoretical FC band. These show that several of the most intense combination bands, often occur at extremely high frequencies relative to the 0–0 band. The FC analysis of the (lowest) 3s Rydberg state (1B_2 symmetry) contains 9730 vibrational states, but only 42 have intensity with molar absorption coefficient (M) greater than $1 \text{ dm}^3 \text{ mol}^{-1} \text{ cm}^{-1}$; many allowed transitions in our previous studies^{2,14} have $10^4 < M < 10^6$.

In contrast, the HT profile in Table VI contains the lowest frequency mode 39 (368 cm^{-1}) of b_2 symmetry. The profile is mainly binary and ternary combination bands, based on the set of FC fundamentals. The whole HT spectrum is stronger than the FC spectrum. The FC profile contains several lower frequencies than the HT one, and is simpler, and hence shown in the figures below. In both Tables V and VI, the peaks occurring with extremely high frequency are the most intense of the whole spectrum, which contains many thousands of vibrational states.

E. Rydberg states identified in the experimental VUV spectrum

We believe that this is the first attempt to identify vibrational structure in the QC absorption spectrum.

We have divided the VUV range of the QC absorption spectrum over the energy range up to 8.8 eV into short sections, as shown in Figs. 5–9; theoretical analyses are superimposed and are discussed below. Figure 5 shows the raw UV + VUV data as A, while the inset (B) shows the regular residuals after fitting a ninth-order polynomial to the curve (A) and plotting the difference data. The full range of these residuals is shown in the supplementary material as SM6; the most prominent detail, from 5.0 to 6.8 eV, was also obtained using a ninth-order polynomial as in the supplementary material as SM7.

Superposition of the Franck–Condon profile for the X^1B_2 3s-Rydberg state, as shown in Fig. 6, leads to a close fit to almost all

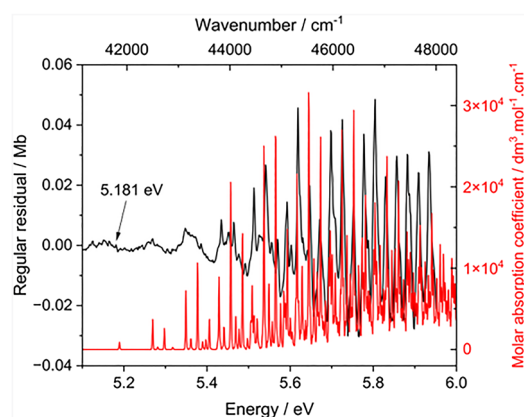


FIG. 5. The onset of very weak structure in the UV absorption of quadricyclane with the Franck–Condon analysis of the 1B_2 state, which defines the lowest 3s-Rydberg state with $n = 3$ and $\delta = 0.932$. The calculated FC have been scaled by 0.97 to bring the principal vibrational sequence into alignment. The band origin is marked with an arrow.

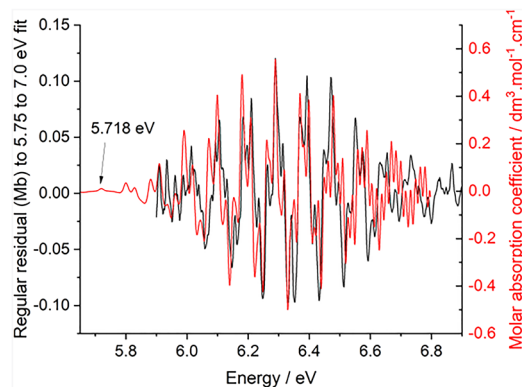


FIG. 6. The 5.7–6.8 eV range of the QC VUV spectrum, with the Franck–Condon profile based on the 1B_2 state 3p-state superimposed. The band origin is shown.

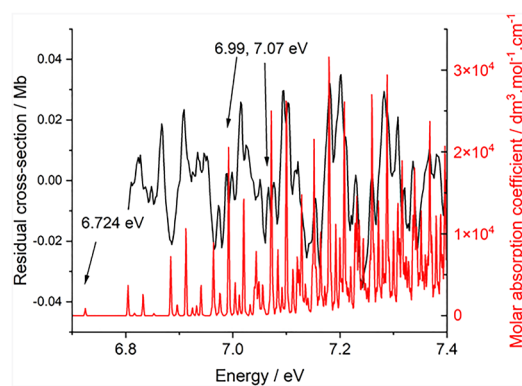


FIG. 7. The 6.7–7.4 eV range of the QC VUV spectrum, with the Franck–Condon profile superimposed; the onset is 6.724 eV and corresponds to a 3d Rydberg state.

the most intense peaks in the range 5.1–6.0 eV. The onset of UV absorption for quadricyclane, after the fit of the spectrum in Fig. 6, is based on the calculated 0–0 band. This same procedure of fitting the main peaks, but using the position of the calculated 0–0 band for the spectral origin was used for the higher energy analyses. We conclude that the 3s-Rydberg state 0–0 band lies at 5.181 eV as shown in Fig. 6. This is 0.26 eV higher than that given by R & W;⁹ however, given the earlier assignment where their AIE was identified with an early VEE, this difference is reasonable.

Our identification of these Rydberg states is cognisant that the R & W assignment⁹ of the binding energies for the 3s and two 3p states is 2.88, 2.29, and 2.24 eV, respectively; these differences are independent of the IE used. The latter pair would be expected to occur in the QC VUV spectrum ~ 0.6 eV higher in energy, close to 5.78 eV.

The energy range above 5.35 eV shows a set of sharp bands up to 5.95 eV and further complex structure from 6.0 to 6.7 eV (Fig. 5, inset). The region from 5.1 to 6.0 eV, shown in Fig. 6, has the FC profile for the 3s Rydberg state superimposed. Almost every peak in

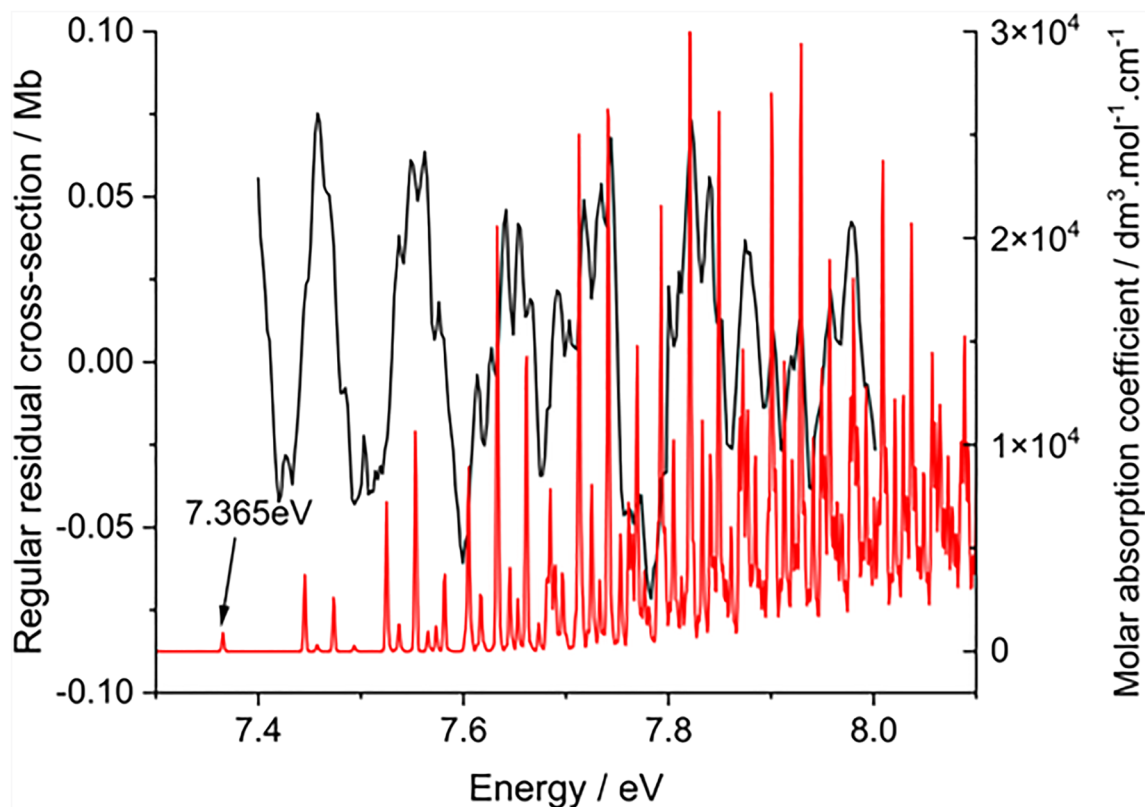


FIG. 8. The 7.3–8.0 eV range of the QC VUV spectrum, with the Franck–Condon profile based on the 4s determination superimposed. The 0–0 band and onset region of the spectrum starts well below the X^2B_2 ionization energy, but the lengthy tail of the spectrum extends into the super-excited state region.

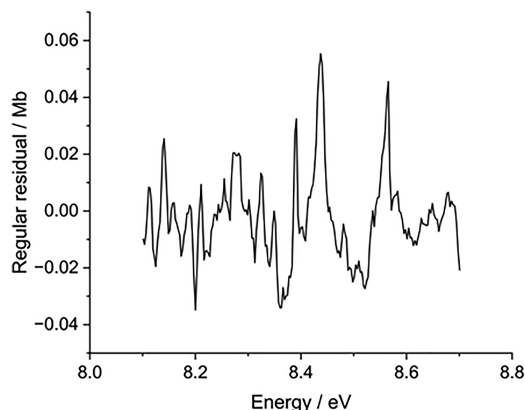


FIG. 9. The range from 8.0 to 8.7 eV, which includes the lowest ionization energy of the QC VUV spectrum and above. These cannot relate to the Rydberg states evident at lower energy.

the region is accounted for although the FC profile does not give a good interpretation of the internal local intensities.

The set of 12 sharp peaks between 5.7 and 5.9 eV, with an average separation close to 212 cm^{-1} over ten intervals, as shown in

Fig. 5, is reminiscent of the VUV spectrum of norbornadiene, where a Rydberg state occurs with similar features. However, in NBD, this is spectroscopic mode 12 (368 cm^{-1}), much larger than the present QC value. Above 6.0 eV, a further set of bands with a more complex profile occurs with a maximum close to 6.290 eV, as shown in Fig. 7. This is the two allowed 3p Rydberg states of 1B_2 and 1A_1 symmetries.

A similar treatment of the spectral range from 5.7 to 6.9 eV gave the black curve in Fig. 7 after fitting both the calculated profile and the spectral data to a further polynomial. A series of FC fits to the region using individual peaks with various half-widths at half-maximum (HWHM) led to the choice of 70 cm^{-1} , which we have often used as the width for an unperturbed state.¹⁴ The fit starting close to 5.8 eV is clearly very similar to the spectrum but diverges slightly above 6.6 eV, which may indicate a further electronic state above that energy. Using the fit to the dense set of peaks allows the 0–0 band of the state at 5.718 eV to be attributed to a 3p Rydberg state.

The next selected region of the VUV spectrum, from 6.8 to 7.4 eV, shown in Figs. 2 and 3, contains weak features on either side of a shallow minimum. Again, a polynomial fit to the raw data for this region exposed fine structure on both sides of the minimum, as shown in Fig. 8. Many of the observed peaks are matched, but in some cases, peaks are doubled, as shown at 6.99 and 7.07 eV. The

super-position of the FC envelope leads to the position of the 0–0 band being at 6.724 eV; this energy corresponds to a 3d Rydberg state, with $n = 3$ with $\delta = 0.136$.

A similar treatment of the next higher energy range from 7.3 to 8.0 eV leads to Fig. 9. This range includes the energy of the X^2B_2 ionic state of QC, previously reported at 7.6706 eV.¹ Thus, the onset in Fig. 9 lies below the ionization energy, while the tail lies in the super-excited state region above the IE.

F. Herzberg–Teller (HT) analyses of the Rydberg states of QC and the impact for ionic states

Vibrational analyses for singlet and triplet states can readily be performed using software such as that from the Pisa group in G-16. Both Franck–Condon and Herzberg–Teller processes are routine. However, ionic states cannot be analyzed by HT processes using these packages owing to incompatibility between the Pisa (vibrational) and Gaussian (equilibrium geometry) codes in G-16 and its predecessors. This arises from the absence of the dipole derivatives being stored on the G-16 checkpoint file, and hence non-availability to the Pisa software. Currently, HT analyses of ionic states are limited to specialist packages, often not available in the public domain. This was the situation when we undertook the vibrational analysis of the photoelectron spectrum of quadricyclane.¹ We believe we have a remedy to this issue.

Rydberg states exhibit the same vibrational profile as their limiting ionic state, at least to first order. Hence, we can determine the HT component of vibrations for the ionic state by the calculation of that for the Rydberg state. We have performed that, here, with significant added information. This results in the contribution of HT vibrations to ionic states via Rydberg states being readily available within G-16 and other suite usage and does not require special techniques.

The HT results, in Table VI for the 3s Rydberg state, are more intense by a factor of 4 than those under FC conditions. However, only one nonsymmetric mode (368 cm^{-1} , b_2) appears. Many of the HT vibrations given in Table VI are combination bands of 368 cm^{-1} with symmetric a_1 vibrations rather than nonsymmetric modes *per se*.

G. Fine structure attributable to valence states

An example from this range of absorption is shown in Fig. 9. Here, all excitation processes lie above the lowest ionization energy, but we have been unable to assign the vibrational structure to a particular state. Using the TDDFT method, but this time with the TZVP basis set, the lowest AEE valence state has the same symmetry (1^1B_2) as the lowest Rydberg state and is predicted to lie between the 3s and 4s Rydberg states, close to 5.803 eV. It shows many similar fundamentals to those for the Rydberg 3s state, but the frequencies are considerably different. A small selection of these valence state frequencies is shown in the supplementary material as SM8 and SM9. The differences from the Rydberg state in Fig. 6 close to the onset are apparent.

IV. CONCLUSIONS

We have presented and analyzed the combined UV + VUV absorption spectrum of quadricyclane for the energy range up to

10.8 eV. The profile does not present any vibrational features but poorly defined broad maxima. The completely σ -bonded structure of the molecule, leading to the absence of a chromophore, is responsible for this appearance. However, by the polynomial fitting of local energy ranges, subtracting from the observed spectral intensity, and plotting the difference spectrum, otherwise known as the regular residuals, we have exposed extensive vibrational structure. Almost every vibration identified by the polynomial subtraction above can be interpreted at the Franck–Condon level for the onset.

The high energy of the σ^* -MOs leads to the onset of the UV spectrum being populated by Rydberg states. Hence, the onset of the UV + VUV spectrum cannot be interpreted by valence state calculations, even when using coupled cluster (SAC-CI) theoretical levels. However, these methods are successful when the Gaussian atomic orbitals (AOs) contain sufficiently diffuse atomic functions to generate Rydberg states; this enables the spectral onset to be interpreted in detail.

Unexpectedly, there is a close correlation between the SAC-CI valence state energies and those determined by the CAM-B3LYP functional. The latter is a much less demanding procedure in computational terms but achieves remarkably similar numerical results.

The Franck–Condon analysis of the spectrum is complex and shows a wide range of intensities, with very weak onsets. This leads to the conclusion that, except for the lowest AEE, there is little chance of the identification of experimental AEE for most Rydberg states unless jet-cooling can be utilized. The FC components of the onset singlet Rydberg state, successfully analyzed above, are overwhelmed at higher energies by Herzberg–Teller states, leading to a loss of spectral definition.

Our study, arguably the largest to date for quadricyclane, shows that the inherent strain energy within the double cyclopropane system can be released, without activation energy, during attempts at the determination of the equilibrium structure for the lowest singlet and triplet states, 1^3A_2 . The result is an excited state of norbornadiene some 6 eV above the ground state. However, several other singlet and triplet states of QC behave normally and generate global minima for equilibrium QC structures.

The Rydberg states generate a profile almost identical to that of the limiting ionic state. Many quantum chemistry suites cannot calculate HT components directly for ionic states. The use of the vibrational profiles for the corresponding Rydberg states provides a simple method of achieving this aim since no special coding is required. This avoids access to dedicated software, often not in the public domain.

We have shown that the determination of Rydberg state energies with spherical harmonics through s, p, d, and f is easily performed. These provide theoretical 0–0 bands, which were used to locate the spectral onsets in the experimental spectrum, that were not apparent in the QC spectrum.

SUPPLEMENTARY MATERIAL

The supplementary material contains additional information on each of the following: 1. SM1. The quadricyclane molecule re-labeled for Rydberg state calculations. 2. SM2. The lowest group

of singlet valence states, determined by the B3LYP method using the Def2-TZVPPD basis set. 3. SM3. The wide scan VUV spectrum with the Def2-TZVPPD basis set using the B3LYP method. SM4. The lowest group of singlet valence states for quadricyclane using the SAC-CI method. SM5. Comparison of the SAC-CI singlet state results with the B3LYP DFT procedure at the 6-311G(d, p) basis set level. SM6. The full range of regular residuals. SM7. The onset polynomial fit to the raw data. Below 5 eV, the two curves are indistinguishable at this scale. SM8. Table SM8 The 1^1B_2 valence state. Calculated onset 0–0 band at 5.8032 eV. Table SM9. The 1^1A_1 valence state. Calculated onset 0–0 band at 6.707 eV.

ACKNOWLEDGMENTS

We thank (a) the ASTRID2 Synchrotron facility, and Aarhus University, for a grant of beam-time, (b) the Italian MIUR (Project No. PON01-010788), and (c) the University of Edinburgh (Eddie3) and Edinburgh Parallel Computing Center (Cirrus) super-computing facilities for support.

AUTHOR DECLARATIONS

Conflict of Interest

The authors have no conflicts to disclose.

Author Contributions

Michael H. Palmer: Conceptualization (equal); Formal analysis (equal); Methodology (equal); Project administration (equal); Supervision (equal); Writing – original draft (equal). **Søren Vronning Hoffmann:** Formal analysis (equal); Resources (equal); Validation (equal); Writing – review & editing (equal). **Nykola C. Jones:** Formal analysis (equal); Investigation (equal); Resources (equal); Supervision (equal); Writing – review & editing (equal). **Marcello Coreno:** Formal analysis (equal); Resources (equal); Validation (equal); Writing – review & editing (equal). **Monica de Simone:** Formal analysis (equal); Funding acquisition (equal); Project administration (equal); Resources (equal); Software (equal); Validation (equal); Writing – review & editing (equal). **Cesare Grazioli:** Formal analysis (equal); Methodology (equal); Resources (equal); Validation (equal); Writing – review & editing (equal). **R. Alan Aitken:** Methodology (equal); Resources (equal); Validation (equal); Writing – review & editing (equal). **Coralyse Peureux:** Investigation (equal); Methodology (equal); Validation (equal); Writing – review & editing (equal).

DATA AVAILABILITY

The data that support the findings of this study are available from the corresponding author upon reasonable request.

APPENDIX: SPECTRAL INTENSITIES

A reviewer has noted that we use three scales of intensity in this study, each for comparability with other work in the field of study. The numerical relationships between these and related units have been previously reported by Cohen and

Taylor³⁵ in Photoabsorption, Photoionization, and Photoelectron Spectroscopy.³⁶

REFERENCES

- 1 M. H. Palmer, M. Coreno, M. de Simone, C. Grazioli, R. A. Aitken, S. V. Hoffmann, N. C. Jones, and C. Peureux, *J. Chem. Phys.* **153**, 204303 (2020).
- 2 M. H. Palmer, S. V. Hoffmann, N. C. Jones, M. Coreno, M. de Simone, C. Grazioli, and R. A. Aitken, *J. Chem. Phys.* **155**, 034308 (2021).
- 3 U. Bauer, L. Fromm, C. Weiß, P. Bachmann, F. Späth, F. Düll, J. Steinhauer, W. Hieringer, A. Görling, A. Hirsch, H.-P. Steinrück, and C. Papp, *J. Phys. Chem. C* **123**, 7654–7664 (2019).
- 4 U. Bauer, L. Fromm, C. Weiß, F. Späth, P. Bachmann, F. Düll, J. Steinhauer, S. Matysik, A. Pominov, A. Görling, A. Hirsch, H.-P. Steinrück, and C. Papp, *J. Chem. Phys.* **150**, 184706 (2019).
- 5 O. Brummel, D. Besold, T. Döpfer, Y. Wu, S. Bochmann, F. Lazzari, F. Waidhas, U. Bauer, P. Bachmann, C. Papp, H.-P. Steinrück, A. Görling, J. Libuda, and J. Bachmann, *ChemSusChem* **9**, 1424 (2016); O. Brummel, F. Waidhas, U. Bauer, Y. Wu, S. Bochmann, H.-P. Steinrück, C. Papp, J. Bachmann, and J. Libuda, *J. Phys. Chem. Lett.* **8**, 2819–2825 (2017).
- 6 A. Valentini, S. van den Wildenberg, and F. Remacle, *Phys. Chem. Chem. Phys.* **22**, 22302–22313 (2020); J. Orrego-Hernández, A. Dreos, and K. Moth-Poulsen, *Acc. Chem. Res.* **53**, 1478–1487 (2020).
- 7 K. Mizuno, T. Fukuyama, and K. Kuchitsu, *Chem. Lett.* **1**, 249–254 (1972); L. Doms, H. J. Geise, C. Van Alsenoy, L. Van Den Eenden, and L. Schäfer, *J. Mol. Struct.* **129**, 299–314 (1985).
- 8 B. Vogelsanger and A. Bauder, *J. Mol. Spectrosc.* **136**, 62–67 (1989).
- 9 F. Rudakov and P. M. Weber, *J. Chem. Phys.* **136**, 134303 (2012).
- 10 H.-D. Martin, C. Heller, E. Haselbach, and Z. Lanyjova, *Helv. Chim. Acta* **57**, 465–472 (1974).
- 11 M. H. Palmer, M. Coreno, M. de Simone, C. Grazioli, S. V. Hoffmann, and N. C. Jones, *J. Chem. Phys.* **150**, 194305 (2019).
- 12 R. O. Ramabhadran and K. Raghavachari, *J. Chem. Theory Comput.* **9**, 3986–3994 (2013).
- 13 M. Lesiuk, *J. Chem. Theory Comput.* **18**, 6537–6556 (2022).
- 14 M. H. Palmer, T. Ridley, S. V. Hoffmann, N. C. Jones, M. Coreno, M. de Simone, C. Grazioli, M. Biczysko, A. Baiardi, and P. Limão-Vieira, *J. Chem. Phys.* **142**, 134302 (2015).
- 15 M. J. Frisch, G. W. Trucks, H. B. Schlegel, G. E. Scuseria, M. A. Robb, J. R. Cheeseman, G. Scalmani, V. Barone, G. A. Petersson, H. Nakatsuji, X. Li, M. Caricato, A. V. Marenich, J. Bloino, B. G. Janesko, R. Gomperts, B. Mennucci, H. P. Hratchian, J. V. Ortiz, A. F. Izmaylov, J. L. Sonnenberg, D. Williams-Young, F. Ding, F. Lipparini, F. Egidi, J. Goings, B. Peng, A. Petrone, T. Henderson, D. Ranasinghe, V. G. Zakrzewski, J. Gao, N. Rega, G. Zheng, W. Liang, M. Hada, M. Ehara, K. Toyota, R. Fukuda, J. Hasegawa, M. Ishida, T. Nakajima, Y. Honda, O. Kitao, H. Nakai, T. Vreven, K. Throssell, J. A. Montgomery, Jr., J. E. Peralta, F. Ogliaro, M. J. Bearpark, J. J. Heyd, E. N. Brothers, K. N. Kudin, V. N. Staroverov, T. A. Keith, R. Kobayashi, J. Normand, K. Raghavachari, A. P. Rendell, J. C. Burant, S. S. Iyengar, J. Tomasi, M. Cossi, J. M. Millam, M. Klene, C. Adamo, R. Cammi, J. W. Ochterski, R. L. Martin, K. Morokuma, O. Farkas, J. B. Foresman, and D. J. Fox, *Gaussian 16*, Revision A.03, Gaussian, Inc., Wallingford, CT, 2016.
- 16 V. Barone, J. Bloino, M. Biczysko, and F. Santoro, *J. Chem. Theory Comput.* **5**, 540–554 (2009).
- 17 J. Bloino, M. Biczysko, F. Santoro, and V. Barone, *J. Chem. Theory Comput.* **6**, 1256–1274 (2010).
- 18 A. Baiardi, J. Bloino, and V. Barone, *J. Chem. Theory Comput.* **9**, 4097–4115 (2013).
- 19 H. Nakatsuji and K. Hirao, *Int. J. Quantum Chem.* **20**, 1301–1313 (1981).
- 20 H. Nakatsuji and T. Yonezawa, *Chem. Phys. Lett.* **87**, 426–431 (1982).
- 21 H. Nakatsuji, *Chem. Phys.* **75**, 425–441 (1983).
- 22 H. Nakatsuji, *Int. J. Quantum Chem.* **24**(S17), 241–255 (1983).
- 23 H. Nakatsuji, K. Ohta, and T. Yonezawa, *J. Phys. Chem.* **87**, 3068–3074 (1983).
- 24 P. Hohenberg and W. Kohn, *Phys. Rev.* **136**, B864–B871 (1964).
- 25 W. Kohn and L. J. Sham, *Phys. Rev.* **140**, A1133–A1138 (1965).

- ²⁶R. G. Parr and W. Yang, *Density-Functional Theory of Atoms and Molecules* (Oxford University Press, Oxford, 1989).
- ²⁷A. D. Becke, *J. Chem. Phys.* **98**, 5648–5652 (1993).
- ²⁸T. Yanai, D. P. Tew, and N. C. Handy, *Chem. Phys. Lett.* **393**, 51–57 (2004).
- ²⁹R. Krishnan, J. S. Binkley, R. Seeger, and J. A. Pople, *J. Chem. Phys.* **72**, 650–654 (1980).
- ³⁰T. H. Dunning, *J. Chem. Phys.* **55**, 716–723 (1971).
- ³¹A. D. McLean and G. S. Chandler, *J. Chem. Phys.* **72**, 5639–5648 (1980).
- ³²R. F. W. Bader, *Acc. Chem. Res.* **18**, 9–15 (1985).
- ³³T. A. Keith, TK Gristmill Software, Overland Park, KS, 2017, AIMQB (Version 14.11.23, Standard), www.aim.tkgristmill.com.
- ³⁴H. S. Yu, X. He, S. L. Li, and D. G. Truhlar, *Chem. Sci.* **7**, 5032–5051 (2016).
- ³⁵E. R. Cohen and B. N. Taylor, *J. Phys. Chem. Ref. Data* **2**, 663 (1973).
- ³⁶*Photoabsorption, Photoionization, and Photoelectron Spectroscopy*, edited by J. Berkowitz (Academic Press, 1979), pp. xv–xviii, ISBN: 978-0124145092.